AGU ADVANCING EARTH AND SPACE SCIENCES

Geophysical Research Letters

RESEARCH LETTER
10.1029/2025GL119404

Reconstructing the Geometry of a Hot Flow Anomaly With Bounding Jets in Magnetosheath

Yufei Zhou[1], Boyi Wang[2], Savvas Raptis[3], Shan Wang[4], Jin Guo[5], Jih-Hong Shue[6], David Sibeck[7], Quanming Lu[5], Jiamei Zhang[1], Chao Shen[1], Rungployphan Kieokaew[8], C. Philippe Escoubet[9], Peng Shao[1,10,11], and James Burch[12]

[1]School of Science, Harbin Institute of Technology (Shenzhen), Shenzhen, China, [2]School of Aerospace Science, Harbin Institute of Technology (Shenzhen), Shenzhen, China, [3]Applied Physics Laboratory, Johns Hopkins University, Laurel, MD, USA, [4]Institute of Space Physics and Applied Technology, Peking University, Beijing, China, [5]School of Earth and Space Sciences, University of Science and Technology of China, Hefei, China, [6]Department of Space Science and Engineering, National Central University, Taoyuan, Taiwan, [7]Goddard Space Flight Center, NASA, Greenbelt, MD, USA, [8]Institut de Recherche en Astrophysique et Planétologie, UPS, CNES, CNRS, Toulouse, France, [9]European Space Research and Technology Centre, European Space Agency (ESA), Noordwijk, The Netherlands, [10]Department of Nuclear Engineering, Yantai University, Yantai, China, [11]Yantai Key Laboratory of Advanced Nuclear Energy Materials and Irradiation Technology, Yantai University, Yantai, China, [12]Space Sector, Southwest Research Institute, San Antonio, TX, USA

Key Points:

- A reconstructed hot flow anomaly (HFA) is shown to be a vast structure, spanning more than 20 R_E across the dayside magnetosheath
- Ground magnetometer data support the reconstruction, confirming the structure's vast scale and its dusk-to-dawn propagation
- One of the HFA bounding jets is exceptionally large, measuring 11 R_E in width and persisting for over 6 min in observation

Supporting Information:

Supporting Information may be found in the online version of this article.

Correspondence to:

C. Shen,
shenchao@hit.edu.cn

Citation:

Zhou, Y., Wang, B., Raptis, S., Wang, S., Guo, J., Shue, J.-H., et al. (2026). Reconstructing the geometry of a hot flow anomaly with bounding jets in magnetosheath. *Geophysical Research Letters*, *53*, e2025GL119404. https://doi.org/10.1029/2025GL119404

Received 12 SEP 2025
Accepted 9 JAN 2026

Author Contributions:

Conceptualization: Yufei Zhou
Data curation: Yufei Zhou, Boyi Wang, Shan Wang
Formal analysis: Yufei Zhou, Boyi Wang, Savvas Raptis, Shan Wang, Jin Guo
Funding acquisition: Yufei Zhou, Chao Shen
Investigation: Yufei Zhou, Boyi Wang, Savvas Raptis, Shan Wang, Jin Guo, Jih-Hong Shue, David Sibeck, Quanming Lu, Jiamei Zhang, Rungployphan Kieokaew, C. Philippe Escoubet, Peng Shao, James Burch
Methodology: Yufei Zhou
Project administration: Yufei Zhou, Chao Shen

Abstract

When interplanetary magnetic field discontinuities interact with planetary bow shocks, hot flow anomalies (HFAs) form in the solar wind and can extend into the magnetosheath. Here we reconstruct the three-dimensional geometry of an HFA bounded by two jet regions in the terrestrial magnetosheath. Using a previously established conceptual model of HFA evolution together with in situ measurements in the magnetosheath and pristine solar wind, we derive the structure's geometrical characteristics and show that its normal aligns with the discontinuity normal. It spans most of the dayside magnetosheath. Ground magnetometer data corroborate the reconstruction, revealing both the scale of the disturbance and its dusk-to-dawn propagation. Notably, one bounding jet reaches 11 R_E in width, significantly larger than the sizes of typical magnetosheath jets reported in the literature.

Plain Language Summary

Hot flow anomalies (HFAs) are explosive disturbances that occur when irregularities in the solar wind hit Earth's bow shock, where the solar wind is decelerated and heated in response to Earth's magnetic obstacle. HFAs have long been thought to be small structures. In this study, we used measurements from multiple spacecraft together with ground-based observations to reconstruct the three-dimensional shape of an HFA in Earth's magnetosheath, the region just outside the geomagnetic field. We found that the disturbance was much larger than expected, stretching across more than 20 Earth radii and covering most of the dayside magnetosheath. Ground magnetometers confirmed both the scale of the disturbance and its movement from dusk to dawn. We also observed a plasma jet at the edge of the HFA that lasted more than 6 min and was far larger than typical jets seen before. These findings show that HFAs can cause global-scale deformations to Earth's magnetic shield.

1. Introduction

Hot flow anomalies (HFAs) are transient structures produced when interplanetary magnetic field discontinuities interact with the bow shock (Turc et al., 2025; Zhang et al., 2022). They feature hot, low-density cores surrounded by compressed magnetic field and plasma (S. J. Schwartz et al., 1985). Heating and deceleration in the core generate downstream pressure gradients that drive sunward magnetosheath flows and localized magnetopause bulging (Sibeck et al., 1998; Šafránková et al., 2002; M. O. Archer et al., 2014), which in turn leads to geomagnetic and auroral responses (Fillingim et al., 2011). The disturbed magnetosheath region can be regarded as the extension of the HFA. HFAs can also accelerate particles to relativistic energies (Liu et al., 2019; Raptis, Lalti, et al., 2025; Turner et al., 2018).

Because they form along the curve where a discontinuity intersects the bow shock, HFAs are elongated parallel to the discontinuity plane (Šafránková et al., 2012), while their perpendicular extent is typically regarded as localized to only a few R_E (S. J. Schwartz et al., 2018; Šafránková et al., 2000; Hasegawa et al., 2012; Sibeck

Resources: Yufei Zhou, Boyi Wang, Savvas Raptis, Shan Wang, Jiamei Zhang
Supervision: Chao Shen
Visualization: Yufei Zhou, Boyi Wang
Writing – original draft: Yufei Zhou
Writing – review & editing: Yufei Zhou, Boyi Wang, Savvas Raptis, Shan Wang, Jin Guo, Jih-Hong Shue, David Sibeck, Quanming Lu, Rungployphan Kieokaew, C. Philippe Escoubet, Peng Shao, James Burch

et al., 2000; Jacobsen et al., 2009; M. O. Archer et al., 2014; Omidi & Sibeck, 2007; Sibeck et al., 1999). HFAs are also observed together with magnetosheath jets (Raptis, Lindberg, et al., 2025; Savin et al., 2012; Zhou et al., 2023, 2024), which appear as transient enhancements of dynamic pressure (Krämer et al., 2024; Plaschke et al., 2018) and may arise from compression and reduced shock deceleration at HFA boundaries (Zhou et al., 2024). Similar signatures of shock discontinuity interactions have been identified upstream of other planetary bow shocks (Collinson et al., 2014; Masters et al., 2009; Uritsky et al., 2014; Valek et al., 2017; Øieroset et al., 2001). A recent study reported a Jovian magnetosheath HFA bounded by two jets (Zhou et al., 2024), thus suggesting that HFAs at other planets can also extend into magnetosheath. However, the absence of pristine solar wind observations prevented the study from reconstructing the three-dimensional structure accurately.

Here we apply a previously established conceptual model of HFA evolution, together with multipoint spacecraft observations at Earth, to reconstruct the geometry of a magnetosheath HFA. We show that the associated disturbance reaches a global scale. In addition to its large extent along the discontinuity plane, it expands substantially in the perpendicular direction, contrary to the conventional view of localized structures. Ground magnetometer observations support the reconstruction, and the results indicate that jets generated by SDI (SDI) can be significantly larger than previously expected.

2. The Conceptual Model

Sibeck et al. (2000) introduced a conceptual model of the SDI process. Here we present a slightly revised version with greater emphasis on geometry.

When a tangential discontinuity intersects the bow shock and the surrounding electric fields point toward the discontinuity, reflected ions from the shock are guided upstream, generating instabilities and heating (Burgess & Schwartz, 1988). The heated region initially forms a wedge that is elongated along the intersection curve between the discontinuity and the bow shock, thickest at the bow shock, and tapers upstream (S. J. Schwartz et al., 2018). Its high thermal pressure drives expansion of the HFA core, compressing the surrounding plasma and producing two bounding layers of enhanced density and magnetic field. This forms a sandwiched wedge structure upstream of the bow shock.

Heating and deceleration within the core establish a pressure gradient in the magnetosheath that drives magnetopause bulging and sunward flows downstream (M. O. Archer et al., 2014). This disturbed region represents the downstream extension of the HFA (see Figure 2a). Compression at the HFA boundaries may generate two bounding shocks connected to the bow shock; because the bounding shocks are nearly tangential to the solar wind flow, they decelerate it inefficiently and create high-speed flows in the downstream. The downstream disturbance therefore maintains the upstream sandwiched structure across the nominal bow shock. Continued expansion of the HFA enhances density in the downstream bounding regions, producing two jet-like regions at the edges of the magnetosheath HFA core.

As the discontinuity convects with the solar wind, its intersection curve with the bow shock sweeps across the shock surface until the two surfaces separate. The HFA moves with this intersection and grows by expanding perpendicular to the discontinuity plane, with its downstream extension enlarging as well. When the discontinuity orientation allows prolonged contact with the bow shock, the HFA and its bounding jets may attain a global scale.

3. Results

3.1. Spacecraft Observation

The Magnetospheric Multiscale (MMS) spacecraft constellation (Burch et al., 2015) crossed the magnetopause at 11:39:00 UTC on 2022-01-30 and remained within the magnetosheath until crossing the bow shock at 13:12:00. Figures 1e–1l show plasma and magnetic field data measured by MMS1 in the magnetosheath. Around 12:30, MMS observed three regions of extreme variations in plasma velocity and dynamic pressure (Figures 1h and 1l). The first and third regions, marked with turquoise shadings, are characterized by high flow speeds comparable to those upstream of the bow shock (not shown), along with high dynamic pressure, 11.9 times the typical magnetosheath and 3.5 times the pristine solar wind value. The flows are supersonic, with peak Mach numbers exceeding 2 (Figure 1j), and thus capable of driving secondary shocks. A slow-flow region with nontrivial sunward flow and low density separated the two jets. The magnetic field rotated substantially across the three regions (Figure 1g). The leading jet, central slow-flow region, and trailing jet persisted for about 80, 270, and

10.1029/2025GL119404

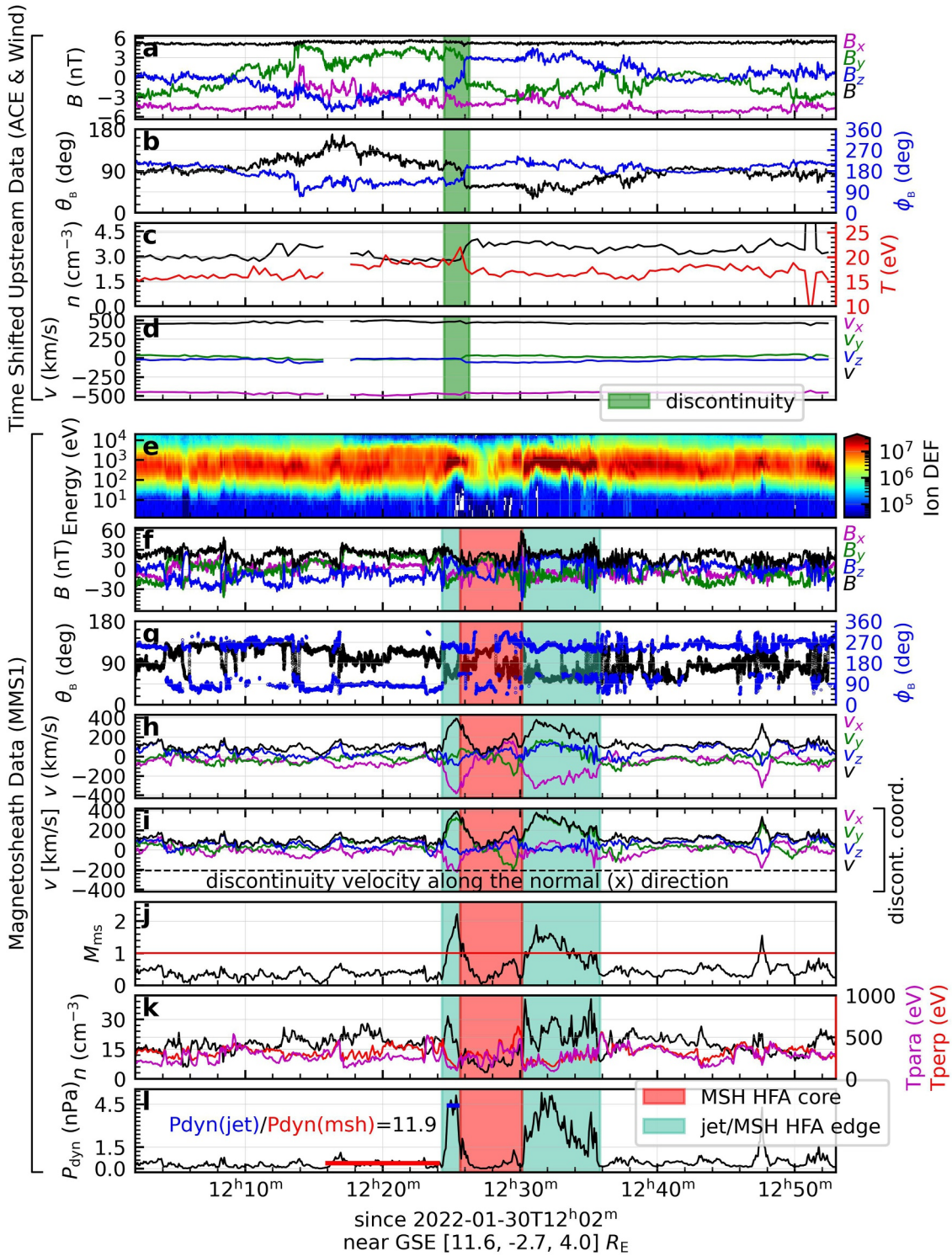

Figure 1. Event overview. The top four panels show time-shifted solar wind data from L1 point to the bow shock nose. The displayed quantities are magnetic field in GSE (a) Cartesian coordinates and (b) spherical coordinates from ACE; ion (c) number density, temperature and (d) bulk velocity from Wind. The following panels show the observation by MMS1, including (e) ion differential energy flux with unit keV · cm^{-2}s^{-1}sr^{-1}keV^{-1}; magnetic field in GSE (f) Cartesian coordinates and (g) spherical coordinates; (h) ion bulk velocity in GSE coordinates; (i) ion bulk velocity in the discontinuity coordinate system in which x direction is along the normal of the discontinuity; (j) magnetosonic number; (k) number density and parallel and perpendicular temperatures; (l) dynamic pressure. Color shadings mark differently interpreted magnetosheath regions.

Table 1
Geometry Reconstruction Parameters

Parameter	Value
Discontinuity MVAB interval	ACE 12:24:30–12:26:20[a]
Discont. min. direction ($\vec{n}$ and $\hat{x}_d$)	(0.40, 0.53, 0.75)[b]
Discont. int. direction ($\hat{y}_d$)	(−0.90, 0.37, 0.22)[b]
Discont. max. direction ($\hat{z}_d$)	(−0.16, −0.76, 0.63)[b]
Discont. MVAB eigenvalue ratio	6.8
Pre-discontinuity interval	ACE and Wind 12:23:30–12:24:30[a]
Post-discontinuity interval	ACE and Wind 12:26:30–12:27:30[a]
$\vec{B}_{pre}$	5.34 (−0.73, 0.65, −0.19) nT
$\vec{B}_{post}$	5.17 (−0.80, −0.23, 0.55) nT
$\vec{n}_{crossB} = \vec{B}_{pre} \times \vec{B}_{post}/\lvert\vec{B}_{pre} \times \vec{B}_{post}\rvert$	(0.32, 0.56, 0.69)
Discont. min direction $\vec{n}$ and $\vec{n}_{crossB}$, $\Delta\theta$	4.9°[c]
$\vec{E}_{pre} = -\vec{v}_{pre} \times \vec{B}_{pre}$	1730 (−0.04, 0.23, 0.97) mV/km
$\vec{E}_{post} = -\vec{v}_{post} \times \vec{B}_{post}$	1724 (−0.02, −0.92, −0.40) mV/km
$\vec{E}_{pre} \cdot \vec{n}$	1,441 mV/km[d]
$\vec{E}_{post} \cdot \vec{n}$	−1,371 mV/km[d]
$\Delta\theta_{EPre,normal}$	34°[d]
$\Delta\theta_{EPost,normal}$	143°[d]
$\vec{v}_{sw} = (\vec{v}_{pre} + \vec{v}_{post})/2$	(−467.4, 10.7, −37.6) km/s
MSH HFA core MVAB interval ($\Delta t_{MSH\ HFA\ core}$)	MMS1 12:25:40–12:30:10 (270 s)[a]
MSH HFA core min. direction	(0.36, 0.57, 0.74)[b]
MSH HFA core int. direction	(−0.84, 0.54, −0.01)[b]
MSH HFA core max. direction	(−0.41, −0.62, 0.67)[b]
MSH HFA core MVAB eigenvalue ratio	3.9
Discont. and MSH HFA core min. direction, $\Delta\theta$	3.0°
discontinuity velocity, $\vec{v}_d = \vec{v}_{sw} \cdot \vec{n}\vec{n}$	−209.0 (0.40, 0.53, 0.75) km/s
Leading jet interval ($\Delta t_{leading\ jet}$)	MMS1 12:24:20–12:25:40 (80 s)[a]
Trailing jet interval ($\Delta t_{trailing\ jet}$)	MMS1 12:30:10–12:35:50 (340 s)[a]
Leading jet width, $w = v_d \cdot \Delta t_{leading\ jet}$	2.6 R_E
MSH HFA core width, $w = v_d \cdot \Delta t_{MSH\ HFA\ core}$	8.8 R_E
Trailing jet width, $w = v_d \cdot \Delta t_{trailing\ jet}$	11.1 R_E

Note. All vectors in the table are given in the GSE coordinate system. [a]ACE UTC+00:50:00, Wind UTC+00:51:40, MMS1 UTC+00:00:00. [b]MVAB applied to the relevant intervals yields the minimum, intermediate, and maximum variance directions of the upstream discontinuity and the magnetosheath HFA core, with the minimum variance direction of the discontinuity representing its normal. [c]The consistency between the minimum variance direction and the magnetic cross product suggests the accurate estimation of the normal. [d]These figures indicate that the motional electric fields at both sides of the discontinuity are directed toward it.

340 s respectively in observation (Table 1), indicating large-scale structures when scaled by the characteristic convection speed in the magnetosheath. The features of the regions are consistent with the conceptual description of a magnetosheath HFA.

Figures 1a–1d show data from two upstream solar wind monitors, ACE and Wind, at the L1 point, after time shifted to account for the propagation from the L1 point to the bow shock. The pristine density, temperature, and velocity (Figures 1c and 1d) were steady, indicating that the extreme dynamic pressures observed in the magnetosheath were not convected with the pristine solar wind but were generated locally at the bow shock, linked to

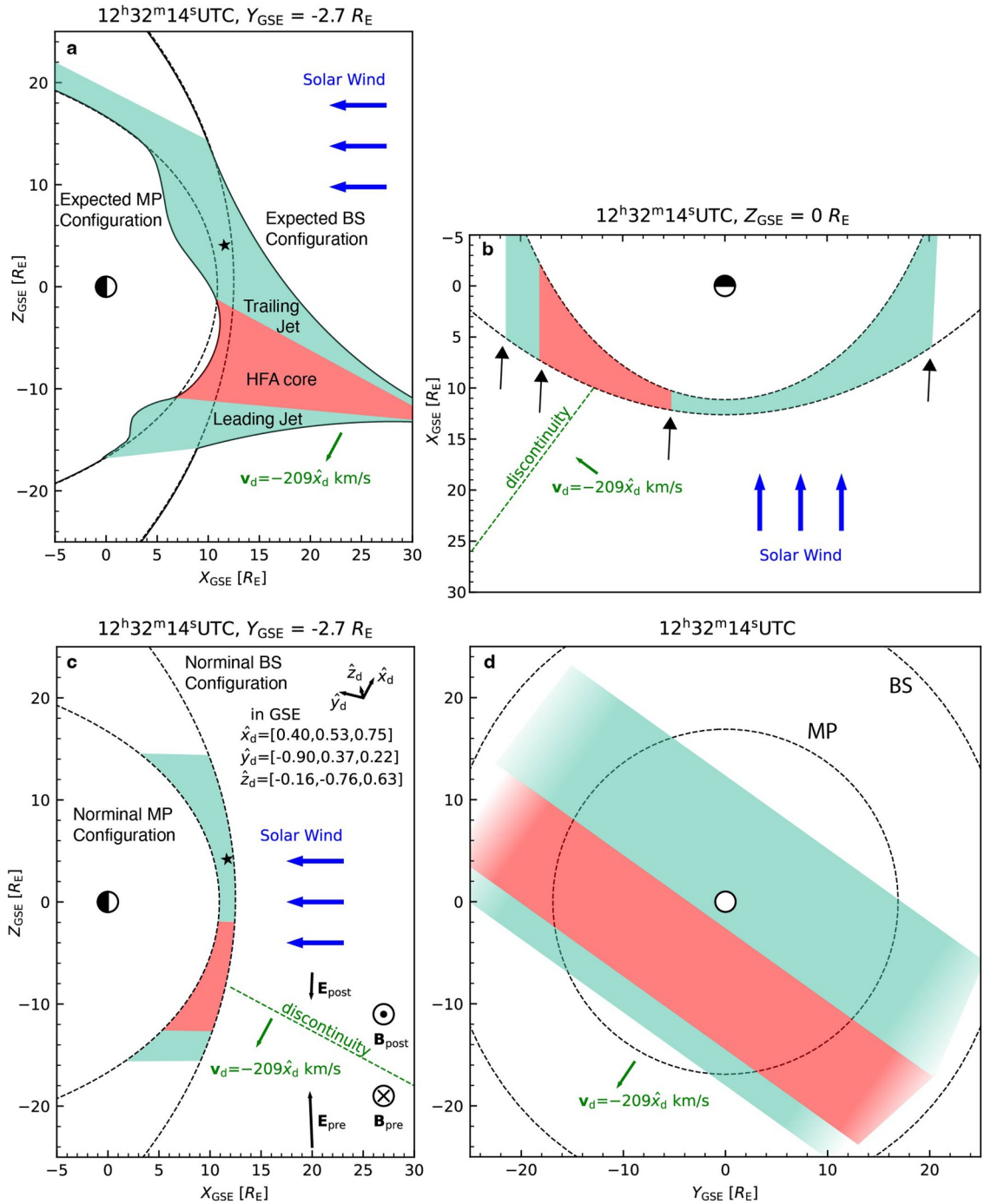

Figure 2. The magnetosheath hot flow anomaly at 12:43:14 UTC as reconstructed from MMS1, ACE, and Wind data. Reconstruction of the spatial size of the disturbances in (c) the $Y_{GSE} = -2.7R_E$ plane and (b) the $Z_{GSE} = 0$ plane, as derived solely from the observational data. Color shadings, as same as in Figure 1, mark different magnetosheath regions. In (d), the disturbances in the $X_{GSE} = 10R_E$ plane is mapped to the terminator plane. In (b), the four black arrows mark the four disturbance boundaries. In (c), The discontinuity is represented by the green dashed line. Black arrows show the motional electric field at two sides of the discontinuity. $\hat{x}_d$ is the normal of the discontinuity. The black star marks the location of Magnetospheric Multiscale (MMS). (a) A schematic showing the expected geometry of the disturbances and boundaries, informed not only by the observational data but also by our understanding of the shock–discontinuity interaction. The disturbance is assumed to propagate with velocity $\vec{v}_d$ while preserving its overall structure as it passed MMS. The magnetopause and bow shock positions are obtained from the Shue98 (Shue et al., 1998) and J05 models (Jeřáb et al., 2005) with parameters $n = 3\text{cm}^{-3}$, $v = 450\text{km/s}$, $B_z = 3\text{nT}$, $B = 5\text{nT}$.

shock dynamics. Marked with green shades in Figures 1a and 1b, the interplanetary magnetic field exhibited a rapid rotation in direction (a magnetic discontinuity) that arrived at the bow shock shortly before MMS observed the three abnormal magnetosheath regions. The magnetic field directions across the upstream discontinuity closely resembled those across the downstream regions (compare Figure 1b with 1g), suggesting a direct relationship between the discontinuity and the formation of the downstream regions.

The discontinuity normal derived from minimum variance analysis of the magnetic field (MVAB) (Bengt U. O. Sonnerup & Scheible, 1998) and from the cross product of the pre- and post-discontinuity magnetic fields are summarized in Table 1. Previous studies suggest that a discontinuity with motional electric fields pointing toward it on at least one side can interact with the bow shock to form an HFA (Burgess & Schwartz, 1988; Thomsen et al., 1993). This condition is satisfied in the present event (Table 1), where the discontinuity is marked by the green dashed line in Figure 2c and the motional electric fields on both sides are directed toward it.

To further correlate the disturbed magnetosheath with the upstream discontinuity, we performed MVAB to determine the three intrinsic orthogonal directions of the HFA core in the magnetosheath (Table 1). The difference between the minimum variance direction of the downstream core and that of the discontinuity is 3.0°. This minimal distinction suggests that the core region downstream is indeed the extension of an upstream HFA. The intermediate and maximum variance directions of the two structures are also closely aligned. Figure 2c illustrates the intrinsic coordinate system of the discontinuity, denoted by $\hat{x}_d$, $\hat{y}_d$, $\hat{z}_d$. The upstream discontinuity has a well-defined normal inferred from its minimum variance direction, supported by the large eigenvalue ratio of 6.8 (Teh, 2025), whereas the downstream disturbance lacks a meaningful normal because it is not a discontinuity.

3.2. The Reconstructed Geometry of Magnetosheath HFA

As the upstream discontinuity propagated with the solar wind, the intersection curve where SDI occurred, together with the resulting HFA and magnetosheath disturbance, moved along the bow shock surface. The time required for the intersection curve to shift from the northern terminator to the southern terminator exceeded 20 min. The duration of the disturbed magnetosheath regions in MMS observation is comparable to this timescale, indicating a large spatial width of the disturbance along the normal direction of the discontinuity.

The comovement of an upstream HFA with its driving discontinuity is commonly used to estimate the HFA width (S. J. Schwartz et al., 2018). The conceptual model (Sibeck et al., 2000) described in Section 2 suggests that the magnetosheath HFA and jets also move together with the discontinuity. Although this comovement will be verified with ground observations in Section 3.3, we here assume it to hold. We also assume trivial expansion of the disturbed regions during spacecraft passage and estimate the width of the regions by

$$w_{\text{region}} = v_d \cdot \Delta t_{\text{region}} \quad (1)$$

where $\vec{v}_d$ is the discontinuity velocity and Δt_{region} is the duration in spacecraft observation (Table 1). Because the regions are elongated along the shock–discontinuity intersection, their widths alone provide sufficient information to reconstruct their three-dimensional structures. The resulting reconstruction is shown from three perspectives in Figures 2c, 2b, and 2d. The disturbance sizes were so large, reaching 30 R_E from south to north and more than 40 R_E from dawn to dusk, that a large portion of the dayside magnetosheath was covered. The minimum size of the disturbance along the discontinuity normal is 22.5 R_E.

Figure 2a shows the expected geometry of the magnetopause and bow shock in the $Y_{GSE} = -2.7\ R_E$ plane, where polar cusps are omitted for simplicity. Since the dynamic pressure in the jet regions reached almost 12 times the nominal magnetosheath value, the magnetopause is expected to be deformed. The bow shock is also anticipated to deform following previous simulations (Lin, 1997, 2002) and the conceptual model (Sibeck et al., 2000).

The jet sizes on a magnetohydrodynamic (MHD) scale and the lower temperatures in the jets are consistent with the interpretation that the jets arise from less efficient deceleration at a curved shock during SDI and from compressions at HFA edges (Hietala et al., 2009; Y. Lin, 2002; Zhou et al., 2023, 2024). Unlike the upstream portions of HFAs, which typically exhibit strong heating and magnetic depressions, such signatures are nearly absent downstream, consistent with their different origins: the upstream HFA is driven directly by SDI, whereas the downstream part forms from magnetosheath outflow (Paschmann et al., 1988). The MHD nature of the

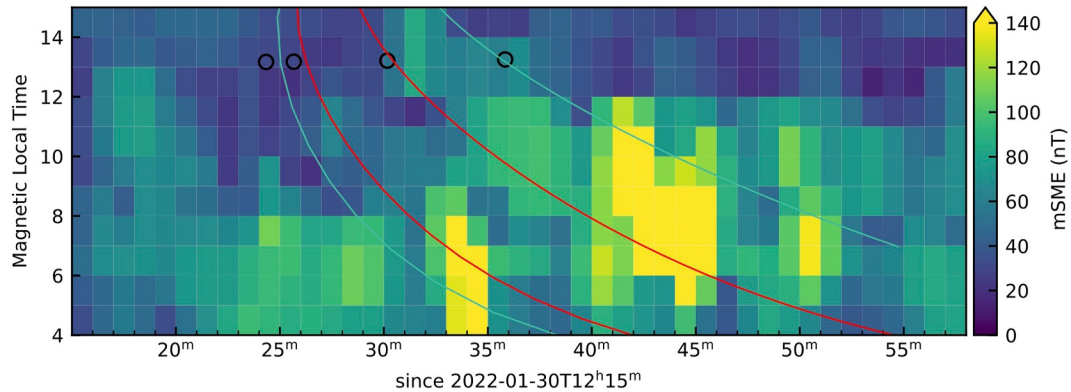

Figure 3. Ground Magnetometer Observations. The color shading indicates the mSME index from 4 to 16 magnetic local time (MLT) during the shock-discontinuity interaction period. Superimposed on the plot are four curves representing the boundaries of the sandwiched structure, as mapped to the ground. The broad band between the rightmost turquoise curve and the adjacent red curve corresponds to the space-time region where a ground response to the trailing jet region (see Figures 2b and 2c) is expected. The region between the two red curves marks the HFA core, while the band between the leftmost turquoise curve and its adjacent red curve represents the leading jet region. Black circles denote the space-time coordinates at which the four boundaries of the sandwiched structure were observed by the Magnetospheric Multiscale spacecraft. The horizontal offsets between these circles and the corresponding projected curves reflect the expected propagation delay of signals from the magnetosheath to the ground.

disturbances is further supported by the Maxwellian ion distributions observed by MMS1 (Figure S2–S3 in Supporting Information S1).

Figure 1i shows ion velocities in the discontinuity coordinate system (see Figure 2c). While the velocities in the jet regions are primarily dominated by the component parallel to the discontinuity (v_y), the leading jet also exhibits a significant normal component (v_x) that matches the convection speed of the upstream discontinuity. Given the MHD nature, this velocity supports the comovement between the magnetosheath disturbance with the upstream discontinuity. Additionally, the sunward anomalous flow along the discontinuity plane is evident in the $v_y < 0$ excursion that reaches -200 km/s within the core region.

The assumption of trivial expansion of the disturbed regions during spacecraft passage potentially leads to underestimated widths of the first jet and the core regions, and thus an overall underestimation of the size of the total disturbance. The flow along the discontinuity normal observed in the leading jet but not in the trailing jet provides some hints of such expansion.

3.3. Ground Observation

A large-scale deformation of the magnetopause produces perturbations in the local magnetic field that can propagate along field lines to the ground (M. Archer et al., 2015; Hietala et al., 2012; Wang et al., 2022, 2024). Consequently, during an SDI event, we expect high-latitude ground magnetometers to record magnetic disturbances over a broad range of dayside magnetic local times (MLT).

Figure 3 presents the local SME index (Newell & Gjerloev, 2014) constructed from 53 SuperMag ground stations at 65°–80°magnetic latitude in the northern hemisphere (see Text S1 in Supporting Information S1 for the station list). The index at a given local time is defined as mSME = mSMU − mSML, where mSMU (mSML) is the maximum (minimum) N-component value within a 3-hr window centered on that local time. The resulting index is displayed as a color map in Figure 3.

To determine the extent of the ground response, we use upstream ACE and Wind measurements together with MMS magnetosheath data to model the dusk–dawn propagation of the shock–discontinuity interaction effects from the bow shock to the ground. In this model, the magnetosheath disturbance propagates from dusk to dawn while expanding at a constant expansion rate, and the disturbance boundaries, as indicated by the four black arrows in Figure 2b, move correspondingly. Knowing the velocities and initial positions of these boundaries from the ACE, Wind and MMS observations, we compute their intersection with the magnetopause as a function of

time. By mapping these intersection points along magnetic field lines to the ground, we obtain the predicted space–time regions of ground perturbations, delineated by turquoise and red curves in Figure 3. See Text S2 in Supporting Information S1 for the detailed calculations.

The wide band between the rightmost turquoise curve and the adjacent red curve corresponds to the expected ground response to the trailing jet region. The band between the leftmost turquoise curve and the adjacent red curve marks the expected response to the leading jet, and the band between the two red curves corresponds to the HFA core. The observed response to the trailing jet falls well within the predicted region, while the response to the leading jet appears broader than expected near 6 MLT, possibly due to changes in flow direction near the flank magnetopause. The overall consistency indicates that the assumed comovement between the upstream discontinuity and the downstream disturbance in our reconstruction is largely valid.

Around UTC 2022-01-30T12:34, which corresponds to Figure 2 with a 2-min delay considering the Alfvénic magnetopause-to-ground propagation (M. Archer et al., 2015), the ground disturbances span from 4 to 15 MLT, covering approximately 8 hr toward dawn and 3 hr toward dusk from local noon. The geomagnetic perturbations last approximately 30 min, consistent with the estimated disturbing duration of over 20 min as the discontinuity sweeps roughly from north to south. Overall, the ground response strengthens after the onset of the interaction.

4. Discussion

While SDIs upstream of the bow shock are well-characterized (S. J. Schwartz et al., 1985; S. J. Schwartz et al., 2018), their global downstream consequences—from magnetosheath to magnetopause—remain less understood despite significant efforts to address this gap (Hasegawa et al., 2012; Jacobsen et al., 2009; M. O. Archer et al., 2014; Raptis, Lindberg, et al., 2025; Sibeck et al., 2000; Šafránková et al., 2002; Eastwood et al., 2008; Chen et al., 2021). An earlier observational study reported a magnetosheath HFA lasting 8 min and producing a large-scale magnetopause deformation parallel to the discontinuity plane (Šafránková et al., 2012), consistent with the view that HFAs extend along the intersection curve between the bow shock and the discontinuity (Sibeck et al., 2000). Two-dimensional hybrid simulations have examined the evolution of magnetosheath HFAs in the plane perpendicular to the discontinuity (Lin, 1997, 2002), revealing propagation and expansion of the downstream disturbance following the upstream HFA and the discontinuity. High speed and high density regions bounding HFA core were also seen in these simulations.

The three-dimensional reconstruction in Figure 2 and the ground observation are consistent with the aggregation of these previous two-dimensional results both parallel and perpendicular to the discontinuity plane. Notably, the disturbance can extend significantly in the perpendicular direction in addition to the anticipated parallel direction, thus occupying a large space in the dayside magnetosheath.

Statistical studies report typical jet durations of ∼30 s in observation and cross-flow scales of ∼1 R_E, with upper limits of 3 min (Plaschke et al., 2018). In contrast, alongside an earlier report of unusually large jets (Gunell et al., 2014), we identify an SDI-generated jet that persists for more than 6 min and spans 11 R_E across. This discrepancy highlights the limitations of statistical criteria, such as a 20-min average of the magnetosheath and solar wind dynamic pressure, and underscores the value of detailed case studies as essential complements to statistical surveys.

The magnetosheath is typically depicted as a homogeneous, stable, and largely static environment on the global scale by its geometrical models, that is the empirical models of magnetopause and bow shock (e.g., Jeřáb et al., 2005; Shue et al., 1998). While these models have been widely used across the studies of the magnetosphere (Němeček et al., 2023), our study suggests large-scale deviation from the static models should occupy a non-trivial period during a day, given that SDI occurs several times a day (Facskó et al., 2008; Zhang et al., 2010) and individual events can persist for tens of minutes depending on the orientation of the discontinuity. The successful prediction of the geomagnetic response from spacecraft data hint toward a path to incorporate the conceptual model of SDI to improve the empirical boundary models.

In addition to tangential discontinuities, simulations have shown that rotational discontinuities can also interact with the bow shock to generate chains of smaller jet. along the discontinuity plane (Lin et al., 1996; Suni et al., 2025). More recently, a simulation has demonstrated that a rotational discontinuity can produce an smaller HFA when assisted by a pre-existing foreshock bubble (Turc et al., 2025). From an observational perspective, it would be valuable to investigate whether such HFAs and associated jets can also attain global scales.

SDI is a universal process that can occur at all planets in the solar system and at exoplanets immersed in supersonic magnetized stellar wind, as upstream HFAs have been observed at Mercury (Uritsky et al., 2014), Venus (Collinson et al., 2014), Mars (Øieroset et al., 2001), Jupiter (Valek et al., 2017), and Saturn (Masters et al., 2009), with downstream disturbances also reported at Jupiter (Zhou et al., 2024). HFAs can grow through temporal expansion (S. Schwartz, 1995), and because the bow shock size at a given planet controls the interaction duration before the discontinuity traverses the shock surface, a scaling between HFA size and bow shock size is expected and supported by observations (Valek et al., 2017). This universality and scaling imply that large-scale magnetosheath disturbances should occur at other planets. Such disturbances, including the jet regions at HFA boundaries, are expected to produce both similar and environment-specific effects. At Mercury, a dynamic-pressure enhancement of 3.5 times the pristine solar wind value can compress the magnetopause by a factor of 1.2, and given its dayside size of only 1.2 planetary radii at perihelion (Winslow et al., 2013), such compression could push the magnetopause to the surface, enabling direct solar wind precipitation. At Mars, increased solar wind dynamic pressure can compress draped and crustal fields, triggering reconnection (Halekas et al., 2009) and driving mass ejection that contributes to atmospheric escape (Ye et al., 2024). At Jupiter, auroral quasi-periodicity on timescales of tens of minutes has been linked to compressional waves in the outer magnetosphere (Yao et al., 2021); although their origin remains uncertain, magnetosheath disturbances may contribute, given the similar timescales at Jupiter (Zhou et al., 2024) and the demonstrated ability of such processes at Earth to excite magnetopause surface waves and compressional waves (M. O. Archer et al., 2019; M. O. Archer et al., 2021; Wang et al., 2020).

One notable feature is that the intrinsic directions of the magnetosheath HFA core closely match those of the discontinuity, as determined by MVAB (Table 1). This consistency suggests that MVAB can be used in planetary magnetosheath studies even when no upstream monitor is available to determine the discontinuity normal.

5. Conclusion

In summary, by combining spacecraft observations in both the pristine solar wind and the magnetosheath with a previously established conceptual model, we estimate the width of an HFA bounded by two jets in the magnetosheath and reconstruct its three-dimensional structure under the assumption that the magnetosheath disturbance is elongated along the discontinuity plane. The result suggests that, in addition to the natural elongation along the discontinuity plane, the disturbance can also extend significantly perpendicular to the discontinuity, due to the expansion of HFA, thereby encompassing much of the dayside magnetosheath. The total width of the disturbance reaches 22.5 R_E. By modeling the dusk-to-dawn propagation of the disturbance using solar-wind and magnetosheath measurements and comparing the results with ground-based observations, we provide further support for this estimated extent and the reconstruction method. Finally, one of the bounding jets persists for more than 6 min and exhibits a minimum cross-flow width of 11 R_E.

Acknowledgments
We thank all people involved in the activities that produced the MMS, ACE, Wind, OMNI, and SuperMag data product and that made the data product publicly available. This work was supported by National Natural Science Foundation of China, Grants 424B2031, 42130202, and 42330202; the National Key Research and Development Program of China, Grant 2022YFA1604600; Shenzhen Technology Project, Grant JCYJ20241202123905008; SR acknowledges support by the Magnetospheric Multiscale (MMS) mission of NASA's Science Directorate Heliophysics Division via subcontract to the Southwest Research Institute (NNG04EB99C). RK acknowledges the postdoctoral fellowship from the French National Space Agency (CNES). This work was also supported by the International Space Science Institute (ISSI) in Bern through the ISSI International Team project no. 556 (cross-scale energy transfer in space plasmas). JG acknowledges support by the Xiaomi Young Talents Program.

Conflict of Interest

The authors declare no conflicts of interest relevant to this study.

Data Availability Statement

The observational data from spacecraft MMS, ACE, and Wind are publicly available at https://cdaweb.gsfc.nasa.gov/. The ground-based magnetometer data is available at https://supermag.jhuapl.edu/.

References

Archer, M., Turner, D., Eastwood, J., Schwartz, S., & Horbury, T. (2015). Global impacts of a foreshock bubble: Magnetosheath, magnetopause and ground-based observations. *Planetary and Space Science*, *106*, 56–66. https://doi.org/10.1016/j.pss.2014.11.026

Archer, M. O., Hartinger, M. D., Plaschke, F., Southwood, D. J., & Rastaetter, L. (2021). Magnetopause ripples going against the flow form azimuthally stationary surface waves. *Nature Communications*, *12*(1), 5697. https://doi.org/10.1038/s41467-021-25923-7

Archer, M. O., Hietala, H., Hartinger, M. D., Plaschke, F., & Angelopoulos, V. (2019). Direct observations of a surface eigenmode of the dayside magnetopause. *Nature Communications*, *10*(1), 615. https://doi.org/10.1038/s41467-018-08134-5

Archer, M. O., Turner, D. L., Eastwood, J. P., Horbury, T. S., & Schwartz, S. J. (2014). The role of pressure gradients in driving sunward magnetosheath flows and magnetopause motion. *Journal of Geophysical Research: Space Physics*, *119*(10), 8117–8125. https://doi.org/10.1002/2014JA020342

Burch, J. L., Moore, T. E., Torbert, R. B., & Giles, B. L. (2015). Magnetospheric multiscale overview and science objectives. *Space Science Reviews*, *199*(1–4), 5–21. https://doi.org/10.1007/s11214-015-0164-9

Burgess, D., & Schwartz, S. J. (1988). Colliding plasma structures: Current sheet and perpendicular shock. *Journal of Geophysical Research*, *93*(A10), 11327–11340. https://doi.org/10.1029/JA093iA10p11327

Chen, L., Ng, J., Omelchenko, Y., & Wang, S. (2021). Magnetopause reconnection and indents induced by foreshock turbulence. *Geophysical Research Letters*, *48*(11), e2021GL093029. https://doi.org/10.1029/2021GL093029

Collinson, G. A., Sibeck, D. G., Masters, A., Shane, N., Zhang, T. L., Fedorov, A., et al. (2014). A survey of hot flow anomalies at Venus. *Journal of Geophysical Research: Space Physics*, *119*(2), 978–991. https://doi.org/10.1002/2013JA018863

Eastwood, J. P., Sibeck, D. G., Angelopoulos, V., Phan, T. D., Bale, S. D., McFadden, J. P., et al. (2008). THEMIS observations of a hot flow anomaly: Solar wind, magnetosheath, and ground-based measurements. *Geophysical Research Letters*, *35*(17), L17S03. https://doi.org/10.1029/2008GL033475

Facskó, G., Kecskeméty, K., Erdős, G., Tátrallyay, M., Daly, P., & Dandouras, I. (2008). A statistical study of hot flow anomalies using cluster data. *Advances in Space Research*, *41*(8), 1286–1291. https://doi.org/10.1016/j.asr.2008.02.005

Fillingim, M., Eastwood, J., Parks, G., Angelopoulos, V., Mann, I., Mende, S., & Weatherwax, A. (2011). Polar uvi and themis gmag observations of the ionospheric response to a hot flow anomaly. *Journal of Atmospheric and Solar-Terrestrial Physics*, *73*(1), 137–145. https://doi.org/10.1016/j.jastp.2010.03.001

Gunell, H., Stenberg Wieser, G., Mella, M., Maggiolo, R., Nilsson, H., Darrouzet, F., et al. (2014). Waves in high-speed plasmoids in the magnetosheath and at the magnetopause. *Annales Geophysicae*, *32*(8), 991–1009. https://doi.org/10.5194/angeo-32-991-2014

Halekas, J. S., Eastwood, J. P., Brain, D. A., Phan, T. D., Øieroset, M., & Lin, R. P. (2009). In situ observations of reconnection hall magnetic fields at mars: Evidence for ion diffusion region encounters. *Journal of Geophysical Research*, *114*(A11), A11204. https://doi.org/10.1029/2009JA014544

Hasegawa, H., Zhang, H., Lin, Y., Sonnerup, B. U. o., Schwartz, S. J., Lavraud, B., & Zong, Q.-G. (2012). Magnetic flux rope formation within a magnetosheath hot flow anomaly. *Journal of Geophysical Research*, *117*(A9), A09214. https://doi.org/10.1029/2012JA017920

Hietala, H., Laitinen, T. V., Andréeová, K., Vainio, R., Vaivads, A., Palmroth, M., et al. (2009). Supermagnetosonic jets behind a collisionless quasiparallel shock. *Physical Review Letters*, *103*(24), 245001. https://doi.org/10.1103/PhysRevLett.103.245001

Hietala, H., Partamies, N., Laitinen, T. V., Clausen, L. B. N., Facskó, G., Vaivads, A., et al. (2012). Supermagnetosonic subsolar magnetosheath jets and their effects: From the solar wind to the ionospheric convection. *Ann. Geophys.*, *30*(1), 33–48. https://doi.org/10.5194/angeo-30-33-2012

Jacobsen, K. S., Phan, T. D., Eastwood, J. P., Sibeck, D. G., Moen, J. I., Angelopoulos, V., et al. (2009). THEMIS observations of extreme magnetopause motion caused by a hot flow anomaly. *Journal of Geophysical Research*, *114*(A8), A08210. https://doi.org/10.1029/2008JA013873

Jeřáb, M., Němeček, Z., Šafránková, J., Jelínek, K., & Měrka, J. (2005). Improved bow shock model with dependence on the IMF strength. *Planetary and Space Science*, *53*(1–3), 85–93. https://doi.org/10.1016/j.pss.2004.09.032

Krämer, E., Koller, F., Suni, J., LaMoury, A. T., Pöppelwerth, A., Glebe, G., & Vörös, Z. (2024). Jets downstream of collisionless shocks: Recent discoveries and challenges. *Space Science Reviews*, *221*(1), 4. https://doi.org/10.1007/s11214-024-01129-3

Lin, Y. (1997). Generation of anomalous flows near the bow shock by its interaction with interplanetary discontinuities. *Journal of Geophysical Research*, *102*(A11), 24265–24281. https://doi.org/10.1029/97JA01989

Lin, Y. (2002). Global hybrid simulation of hot flow anomalies near the bow shock and in the magnetosheath. *Planetary and Space Science*, *50*(5–6), 577–591. https://doi.org/10.1016/S0032-0633(02)00037-5

Lin, Y., Swift, D. W., & Lee, L. C. (1996). Simulation of pressure pulses in the bow shock and magnetosheath driven by variations in interplanetary magnetic field direction. *Journal of Geophysical Research*, *101*(A12), 27251–27269. https://doi.org/10.1029/96JA02733

Liu, T. Z., Angelopoulos, V., & Lu, S. (2019). Relativistic electrons generated at earth's quasi-parallel bow shock. *Science Advances*, *5*(7), eaaw1368. https://doi.org/10.1126/sciadv.aaw1368

Masters, A., McAndrews, H. J., Steinberg, J. T., Thomsen, M. F., Arridge, C. S., Dougherty, M. K., et al. (2009). Hot flow anomalies at saturn's bow shock. *Journal of Geophysical Research*, *114*(A8), A08217. https://doi.org/10.1029/2009JA014112

Němeček, Z., Šafránková, J., Grygorov, K., Mokrý, A., Pi, G., Aghabozorgi Nafchi, M., et al. (2023). Extremely distant magnetopause locations caused by magnetosheath jets. *Geophysical Research Letters*, *50*(24), e2023GL106131. https://doi.org/10.1029/2023GL106131

Newell, P. T., & Gjerloev, J. W. (2014). Local geomagnetic indices and the prediction of auroral power. *Journal of Geophysical Research: Space Physics*, *119*(12), 9790–9803. https://doi.org/10.1002/2014JA020524

Øieroset, M., Mitchell, D. L., Phan, T. D., Lin, R. P., & Acuña, M. H. (2001). Hot diamagnetic cavities upstream of the martian bow shock. *Geophysical Research Letters*, *28*(5), 887–890. https://doi.org/10.1029/2000GL012289

Omidi, N., & Sibeck, D. G. (2007). Formation of hot flow anomalies and solitary shocks. *Journal of Geophysical Research*, *112*(A1), A01203. https://doi.org/10.1029/2006JA011663

Paschmann, G., Haerendel, G., Sckopke, N., Möbius, E., Lühr, H., & Carlson, C. W. (1988). Three-dimensional plasma structures with anomalous flow directions near the earth's bow shock. *Journal of Geophysical Research*, *93*(A10), 11279–11294. https://doi.org/10.1029/JA093iA10p11279

Plaschke, F., Hietala, H., Archer, M., Blanco-Cano, X., Kajdič, P., Karlsson, T., et al. (2018). Jets downstream of collisionless shocks. *Space Science Reviews*, *214*(5), 81. https://doi.org/10.1007/s11214-018-0516-3

Raptis, S., Lalti, A., Lindberg, M., Turner, D. L., Caprioli, D., & Burch, J. L. (2025). Revealing an unexpectedly low electron injection threshold via reinforced shock acceleration. *Nature Communications*, *16*(1), 488. https://doi.org/10.1038/s41467-024-55641-9

Raptis, S., Lindberg, M., Liu, T. Z., Turner, D. L., Lalti, A., Zhou, Y., et al. (2025). Multimission observations of relativistic electrons and high-speed jets linked to shock-generated transients. *The Astrophysical Journal Letters*, *981*(1), L10. https://doi.org/10.3847/2041-8213/adb154

Šafránková, J., Goncharov, O., Němeček, Z., Přech, L., & Sibeck, D. G. (2012). Asymmetric magnetosphere deformation driven by hot flow anomaly(ies). *Geophysical Research Letters*, *39*(15), L15107. https://doi.org/10.1029/2012GL052636

Šafránková, J., Přech, L., Němeček, Z., & Sibeck, D. (2002). The structure of hot flow anomalies in the magnetosheath. *Advances in Space Research*, *30*(12), 2737–2744. https://doi.org/10.1016/S0273-1177(02)80398-2

Šafránková, J., Přech, L., Němeček, Z., Sibeck, D. G., & Mukai, T. (2000). Magnetosheath response to the interplanetary magnetic field tangential discontinuity. *Journal of Geophysical Research*, *105*(A11), 25113–25121. https://doi.org/10.1029/1999JA000435

Savin, S., Amata, E., Zelenyi, L., Lutsenko, V., Safrankova, J., Nemecek, Z., et al. (2012). Super fast plasma streams as drivers of transient and anomalous magnetospheric dynamics. *Ann. Geophys.*, *30*(1), 1–7. https://doi.org/10.5194/angeo-30-1-2012

Schwartz, S. (1995). Hot flow anomalies near the earth's bow shock. *Advances in Space Research*, *15*(8–9), 107–116. https://doi.org/10.1016/0273-1177(94)00092-F

Schwartz, S. J., Avanov, L., Turner, D., Zhang, H., Gingell, I., Eastwood, J. P., et al. (2018). Ion kinetics in a hot flow anomaly: MMS observations. *Geophysical Research Letters*, *45*(21), 529. https://doi.org/10.1029/2018GL080189

Schwartz, S. J., Chaloner, C. P., Christiansen, P. J., Coates, A. J., Hall, D. S., Johnstone, A. D., et al. (1985). An active current sheet in the solar wind. *Nature*, *318*(6043), 269–271. https://doi.org/10.1038/318269a0

Shue, J.-H., Song, P., Russell, C. T., Steinberg, J. T., Chao, J. K., Zastenker, G., et al. (1998). Magnetopause location under extreme solar wind conditions. *Journal of Geophysical Research*, *103*(A8), 17691–17700. https://doi.org/10.1029/98JA01103

Sibeck, D. G., Borodkova, N. L., Schwartz, S. J., Owen, C. J., Kessel, R., Kokubun, S., et al. (1999). Comprehensive study of the magnetospheric response to a hot flow anomaly. *Journal of Geophysical Research*, *104*(A3), 4577–4593. https://doi.org/10.1029/1998JA900021

Sibeck, D. G., Borodkova, N. L., Zastenker, G. N., Romanov, S. A., & Sauvaud, J.-A. (1998). Gross deformation of the dayside magnetopause. *Geophysical Research Letters*, *25*(4), 453–456. https://doi.org/10.1029/98GL00134

Sibeck, D. G., Kudela, K., Lepping, R. P., Lin, R., Nemecek, Z., Nozdrachev, M. N., et al. (2000). Magnetopause motion driven by interplanetary magnetic field variations. *Journal of Geophysical Research*, *105*(A11), 25155–25169. https://doi.org/10.1029/2000JA900109

Sonnerup, B. U. O., & Scheible, M. (1998). Minimum and maximum variance analysis. In G. Paschmann & P. W. Daly (Eds.), *Analysis methods for multi-spacecraft data* (p. 185). ESA Publications Division.

Suni, J., Palmroth, M., Turc, L., Battarbee, M., Pfau-Kempf, Y., & Ganse, U. (2025). Magnetosheath jets associated with a solar wind rotational discontinuity in a hybrid-vlasov simulation. *Journal of Geophysical Research: Space Physics*, *130*(6), e2025JA033995. https://doi.org/10.1029/2025JA033995

Teh, W.-L. (2025). Analytical insights into inaccurate normal vector determination by minimum variance analysis of magnetic fields. *The Astrophysical Journal*, *982*(1), 2. https://doi.org/10.3847/1538-4357/adb847

Thomsen, M. F., Thomas, V. A., Winske, D., Gosling, J. T., Farris, M. H., & Russell, C. T. (1993). Observational test of hot flow anomaly formation by the interaction of a magnetic discontinuity with the bow shock. *Journal of Geophysical Research*, *98*(A9), 15319–15330. https://doi.org/10.1029/93JA00792

Turc, L., Archer, M. O., Zhou, H., Pfau-Kempf, Y., Suni, J., Kajdič, P., et al. (2025). Interplay between a foreshock bubble and a hot flow anomaly forming along the same rotational discontinuity. *Geophysical Research Letters*, *52*(12), e2025GL116473. https://doi.org/10.1029/2025GL116473

Turner, D. L., Wilson, L. B., Liu, T. Z., Cohen, I. J., Schwartz, S. J., Osmane, A., et al. (2018). Autogenous and efficient acceleration of energetic ions upstream of earth's bow shock. *Nature*, *561*(7722), 206–210. https://doi.org/10.1038/s41586-018-0472-9

Uritsky, V. M., Slavin, J. A., Boardsen, S. A., Sundberg, T., Raines, J. M., Gershman, D. J., et al. (2014). Active current sheets and candidate hot flow anomalies upstream of mercury's bow shock. *Journal of Geophysical Research: Space Physics*, *119*(2), 853–876. https://doi.org/10.1002/2013JA019052

Valek, P. W., Thomsen, M. F., Allegrini, F., Bagenal, F., Bolton, S., Connerney, J., et al. (2017). Hot flow anomaly observed at jupiter's bow shock. *Geophysical Research Letters*, *44*(16), 8107–8112. https://doi.org/10.1002/2017GL073175

Wang, B., Liu, J., Han, D., Wang, Y., & Feng, X. (2024). Statistical study of hot flow anomaly induced ground magnetic ultra-low frequency oscillations. *Journal of Geophysical Research: Space Physics*, *129*(8), e2024JA032667. https://doi.org/10.1029/2024JA032667

Wang, B., Liu, T., Nishimura, Y., Zhang, H., Hartinger, M., Shi, X., et al. (2020). Global propagation of magnetospheric pc5 ulf waves driven by foreshock transients. *Journal of Geophysical Research: Space Physics*, *125*(12), e2020JA028411. https://doi.org/10.1029/2020JA028411

Wang, B., Nishimura, Y., Hietala, H., & Angelopoulos, V. (2022). Investigating the role of magnetosheath high-speed jets in triggering dayside ground magnetic ultra-low frequency waves. *Geophysical Research Letters*, *49*(22), e2022GL099768. https://doi.org/10.1029/2022GL099768

Winslow, R. M., Anderson, B. J., Johnson, C. L., Slavin, J. A., Korth, H., Purucker, M. E., et al. (2013). Mercury's magnetopause and bow shock from messenger magnetometer observations. *Journal of Geophysical Research: Space Physics*, *118*(5), 2213–2227. https://doi.org/10.1002/jgra.50237

Yao, Z., Dunn, W. R., Woodfield, E. E., Clark, G., Mauk, B. H., Ebert, R. W., et al. (2021). Revealing the source of jupiter's x-ray auroral flares. *Science Advances*, *7*(28), eabf0851. https://doi.org/10.1126/sciadv.abf0851

Ye, Y., Xu, X., Lee, L.-C., Yu, J., Wang, J., Zhu, B., et al. (2024). In situ observation of mass ejections caused by magnetic reconnections in the ionosphere of mars. *Nature Astronomy*, *8*(7), 838–845. https://doi.org/10.1038/s41550-024-02254-3

Zhang, H., Sibeck, D. G., Zong, Q.-G., Gary, S. P., McFadden, J. P., Larson, D., et al. (2010). Time history of events and macroscale interactions during substorms observations of a series of hot flow anomaly events. *Journal of Geophysical Research*, *115*(A12), A12235. https://doi.org/10.1029/2009JA015180

Zhang, H., Zong, Q., Connor, H., Delamere, P., Facskó, G., Han, D., et al. (2022). Dayside transient phenomena and their impact on the magnetosphere and ionosphere. *Space Science Reviews*, *218*(5), 40. https://doi.org/10.1007/s11214-021-00865-0

Zhou, Y., Raptis, S., Wang, S., Shen, C., Ren, N., & Ma, L. (2024). Magnetosheath jets at jupiter and across the solar system. *Nature Communications*, *15*(1), 4–8. https://doi.org/10.1038/s41467-023-43942-4

Zhou, Y., Shen, C., & Ji, Y. (2023). Undulated shock surface formed after a shock–discontinuity interaction. *Geophysical Research Letters*, *50*(10), e2023GL103848. https://doi.org/10.1029/2023GL103848

References From the Supporting Information

King, J. H., & Papitashvili, N. E. (2005). Solar wind spatial scales in and comparisons of hourly wind and ace plasma and magnetic field data. *Journal of Geophysical Research*, *110*(A2), A02104. https://doi.org/10.1029/2004JA010649

Lepping, R. P., Acũna, M. H., Burlaga, L. F., Farrell, W. M., Slavin, J. A., Schatten, K. H., et al. (1995). The WIND magnetic field investigation. *Space Science Reviews*, *71*(1–4), 207–229. https://doi.org/10.1007/BF00751330

Lin, R. P., Anderson, K. A., Ashford, S., Carlson, C., Curtis, D., Ergun, R., et al. (1995). A three-dimensional plasma and energetic particle investigation for the wind spacecraft. *Space Science Reviews*, *71*(1–4), 125–153. https://doi.org/10.1007/BF00751328

McComas, D. J., Bame, S. J., Barker, P., Feldman, W. C., Phillips, J. L., Riley, P., & Griffee, J. W. (1998). Solar wind electron proton alpha monitor (swepam) for the advanced composition explorer. *Space Science Reviews*, *86*(1), 563–612. https://doi.org/10.1023/A:1005040232597

Pollock, C., Moore, T., Jacques, A., Burch, J., Gliese, U., Saito, Y., et al. (2016). Fast plasma investigation for magnetospheric multiscale. *Space Science Reviews*, *199*(1–4), 331–406. https://doi.org/10.1007/s11214-016-0245-4

Russell, C. T., Anderson, B. J., Baumjohann, W., Bromund, K. R., Dearborn, D., Fischer, D., et al. (2014). The magnetospheric multiscale magnetometers. *Space Science Reviews*, *199*(1–4), 189–256. https://doi.org/10.1007/s11214-014-0057-3

Smith, C. W., L'Heureux, J., Ness, N. F., Acuña, M. H., Burlaga, L. F., & Scheifele, J. (1998). The ace magnetic fields experiment. *Space Science Reviews*, *86*(1), 613–632. https://doi.org/10.1023/A:1005092216668